

# Neutrinos from propagation of ultra–high energy protons

Ralph Engel & Todor Stanev

*Bartol Research Institute, University of Delaware, Newark, DE 19716, USA*

We present a calculation of the production of neutrinos during propagation of ultra-high energy cosmic rays from their astrophysical sources to us. Photoproduction interactions are modeled with the event generator SOPHIA that represents very well the experimentally measured particle production cross sections at accelerator energies. We give the fluxes expected from different assumptions on cosmic ray source distributions, cosmic ray injection spectra, cosmological evolution of the sources and different cosmologies, and compare them to the Waxman-Bahcall limit on source neutrinos. The ratio of the local high energy neutrino flux to the ultra-high energy cosmic ray flux is a crucial parameter in distinguishing between astrophysical and cosmological (top-down) scenarios of the ultra-high energy cosmic ray origin.

98.70.Sa, 13.85Tp, 98.80.Es, 13.15.+g

## I. INTRODUCTION

The highest energy cosmic rays are energetic enough to have photoproduction interactions on the microwave background. These collisions cause energy loss affecting the cosmic rays spectrum [1] – the GZK cutoff. In most astrophysical environments all secondary mesons produced in photoproduction interactions decay into  $\gamma$ -rays and neutrinos. Shortly after the original papers on the GZK cutoff it was suggested [2] that guaranteed fluxes of ultra-high energy (UHE) neutrinos will be produced by the propagation of UHE cosmic ray (UHECR) protons in the Universe. This suggestion was followed by more sophisticated estimates [3–7] that attempted to predict more realistically the expected neutrino fluxes and relate the detection of such fluxes to the neutrino cross section at very high energy and the then unknown mass of the  $W$  boson. Hill & Schramm [8,9] introduced the cosmological evolution of the cosmic rays sources and used the measurements of the cosmic ray spectrum by the Haverah Park [10] and the Fly’s Eye [11] experiments to determine minimum and maximum allowed normalizations for the flux of such ‘propagation’ neutrinos and calculated detection rates for different types of detectors. More recent estimates include the work of Stecker and collaborators [12] and Yoshida & Teshima [13].

Meanwhile the world statistics of ultra-high energy cosmic rays was significantly increased [14] and, most importantly, two events of energy substantially above  $10^{20}$  eV were detected by the Fly’s Eye [15] and AGASA [16] experiments. These events suggest that the maximum energy of cosmic ray acceleration  $E_{max}$  may be significantly higher than the previous nominal estimate of  $10^{20}$  eV, if these events are not a result of the decay of extremely massive exotic particles [17].

We assume that UHECR are of astrophysical origin and present here a new estimate of the expected neutrino fluxes generated during propagation by the ultra-high energy cosmic rays. We use recent results on the propaga-

tion of UHE protons [18] to estimate the neutrino production. The aim is to explore the neutrino production with a photoproduction interaction model (SOPHIA [19]) that fits well the experimentally measured multiparticle production data over a wide energy range. For this purpose we extend the calculation of proton propagation in the local universe by Stanev *et al.* [18] to cosmological distances. We also study the importance of the cosmological evolution of the sources of cosmic rays in different cosmological models. The aim of the present work is to study the level at which these ultra-high energy neutrinos are indeed guaranteed.

In Section 2 we introduce the relevant features of the photoproduction model and discuss the conditions under which the proton propagation calculation was performed. Section 3 discusses the neutrino production from propagation of ultra-high energy protons in the local Universe. In Section 4 we obtain the neutrino spectra from homogeneously distributed cosmic ray sources accounting for the cosmological evolution of these sources. We also test the influence of different proton injection spectra and possible local UHECR sources on the expected neutrino fluxes. Section 5 gives a brief overview of the event rates that could be expected in future large neutrino detectors. Discussion of the results and the conclusions from this research are given in Section 6.

## II. COSMIC RAY PROPAGATION IN THE LOCAL UNIVERSE

In the following we summarize the method of calculating proton propagation in the nearby universe (for a detailed discussion see [18]). The extension of this method to cosmological distances is discussed Sec. IV.

The calculation is carried out as a Monte Carlo simulation of individual particle trajectories in the presence of a random magnetic field. In a first step a turbulent magnetic field is sampled within an effective volume of  $128 \times 8 \times 8$  Mpc. The wave number spectrum of the field strength is assumed to satisfy a Kolmogorov distribution with  $\langle |\vec{B}| \rangle = 1$  nG. Periodic boundary conditions are imposed if a particle trajectory leaves the vol-

ume of pre-calculated magnetic field configurations. The particle's equations of motion are integrated by simulating proton-initiated trajectories according to the ambient magnetic field, including energy loss processes such as photoproduction,  $e^+e^-$  pair production, and adiabatic losses. The protons are injected at the origin of the local coordinate system and the trajectories are calculated until they reach a distance  $R$  from injection point,  $R$  being typically up to 200 Mpc. The observer is thus on a sphere of radius  $R$ . The redshift along the trajectories is approximately calculated using the proper distance-redshift relation with  $z = 0$  on the sphere.

An important new ingredient of this calculation is the detailed simulation of proton/neutron scattering off photons from the cosmic microwave background which is done with the event generator SOPHIA [19]. This event generator has several main differences from previously used codes:

(1) the representation of direct pion production at the photoproduction threshold - a process that only generates charged pions. In terms of Feynman graphs, this process has a strong vertex at the baryon branch and an electromagnetic vertex for the photon interaction. The presence of the electromagnetic vertex requires that the particle the nucleon couples to is charged. Although the cross section for this process is smaller than the dominant  $\Delta^+$  resonance, it yields a significant number of neutrinos, when folded with the steep proton injection spectrum.

(2) explicit consideration of 10 different resonance production channels in the important energy region just above the particle production threshold.

(3) QCD motivated multipion production at large center-of-mass energies - this improvement will not be very important for interactions of the steep cosmic ray spectrum on microwave background, but can have influence for hard photon spectra.

The good representation of the photoproduction cross section as a function of energy becomes very important in proton propagation over distances exceeding the mean free path for photoproduction, when protons suffer multiple collisions on the microwave background. We will demonstrate the effect further down, when our results are compared to previous work.

We consider in the following power-law source spectra with an exponential high-energy cutoff

$$\frac{dN}{dE} \propto E^{-2} \times \exp(-E/E_{max}) \quad (1)$$

and  $E_{max} = 10^{21.5}$  eV. Practically, protons are injected on a  $E^{-2}$  spectrum in narrow logarithmic bins (10 bins per energy decade) and all products of their interactions are collected with the same energy binning. The injection energy ranges from  $10^{19}$  to  $10^{22}$  eV. This gives the option to explore different injection power spectra and cutoff energies by rescaling the products of each energy bin. All neutrinos produced in photoproduction interactions are red-shifted according to the distance of the interaction

point from Earth at  $z = 0$ . The energy loss of the protons due to the expansion of the universe is calculated using  $H_0 = 75$  km/s/Mpc.

### III. NEUTRINO FLUXES FROM PROTON PROPAGATION IN THE LOCAL UNIVERSE

The energy degradation of ultra-high energy protons in propagation in the microwave background is very fast. The minimum mean free path for photoproduction interactions is 3.8 Mpc at a proton energy of  $\sim 6 \times 10^{20}$  eV. Protons with an energy of about  $10^{21}$  eV thus interact on the average twice or more during the first 10 Mpc of propagation and lose close to 50% of their injection energy. A significant fraction of the energy loss (about 40%) goes into neutrinos. The neutrino flux thus originates from the initial stages of proton propagation.

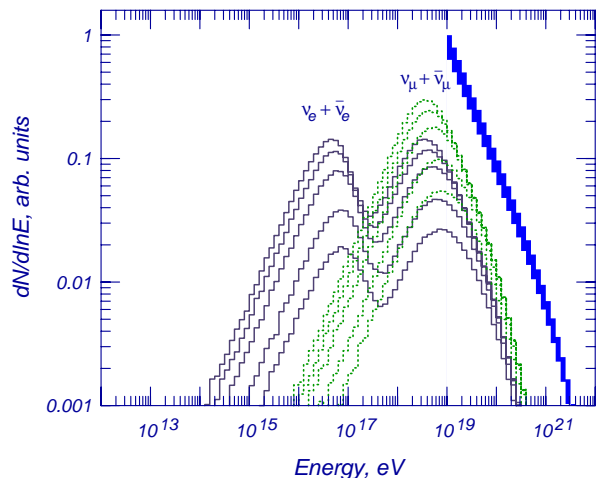


FIG. 1. Neutrino fluxes produced during the propagation of protons over 10, 20, 50, 100, and 200 Mpc (from bottom up) in a 1 nG random magnetic field. The heavy histogram shows the proton injection spectrum defined in Eq. (1).

Fig. 1 shows the fluxes of electron and muon neutrinos after propagation over different distances up to a maximum of 200 Mpc. About 60% of the final neutrino fluxes are generated in the first 50 Mpc and more than 80% - in the first 100 Mpc. The contribution from the second half of the maximum propagation distance is small because the proton spectrum is deprived of  $> 10^{20}$  eV particles and photoproduction interactions are rare.

There are two other noticeable features in the neutrino spectra shown in Fig. 1. The muon neutrino spectra have a single peak at energies between  $10^{18}$  and  $10^{19}$  eV. Electron neutrinos, however, exhibit a more complicated double peak structure. The first peak between  $10^{16}$  and  $10^{17}$  eV is populated by  $\bar{\nu}_e$  from neutron decay. The neutron decay length equals the photoproduction interaction length at about  $4 \times 10^{20}$  eV and neutrons of lower energy are more likely to decay than to interact. This

leads to the formation an additional peak in the electron neutrino spectrum. The second peak, in a position similar to that of muon neutrinos, is populated mostly by  $\nu_e$  from  $\mu^+$  decay with a small admixture of  $\bar{\nu}_e$  generated predominantly in neutron photoproduction interactions. The ratio of  $(\nu_\mu + \bar{\nu}_\mu)/(\nu_e + \bar{\nu}_e)$  in the second peak is 2, as expected, although integrated over the whole spectrum the ratio is closer to 1.

One also notices the slight shift of the peak of the distribution to lower energy with the propagation distance. At longer propagation distance, especially when accounting for the proton scattering in the intergalactic magnetic fields, lower energy protons suffer photoproduction interactions and generate lower energy neutrinos. There is also a small effect from the adiabatic losses of all neutrinos, which is hardly noticeable here because of the small maximum redshift.

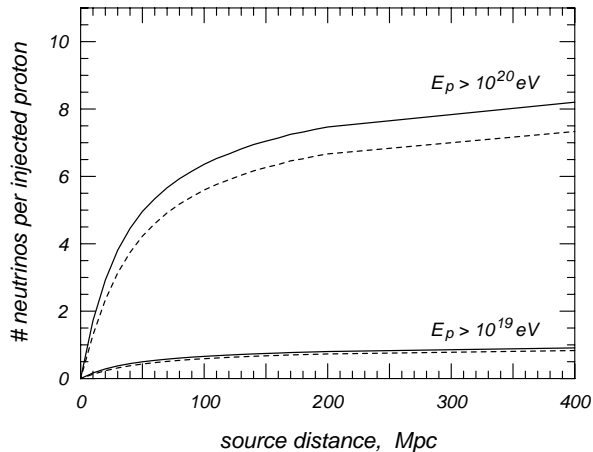


FIG. 2. Total number of neutrinos produced per injected proton of energy above  $10^{19}$  eV (lower set) and  $10^{20}$  eV. The proton energy was sampled from the spectrum (1). Solid lines show the sum of muon neutrinos and antineutrinos, the dashed lines are for electron neutrinos and antineutrinos.

Fig. 2 shows the total number of neutrinos produced per source proton as a function of the source distance. Because the protons lose most of their energy during propagation over the first 50 Mpc, one would naively expect that the neutrino number does not change for source distances above 100 Mpc. The continuing rise of the neutrino to proton number ratio is due to redshift effects. The minimum proton energy for photoproduction interactions decreases as  $(1+z)^{-1}$ , which leads to an increase of the number of interacting protons. Even for relatively small redshifts involved ( $z = 0.1$  for 400 Mpc) this leads to an increase of the generated number of neutrinos.

Fig. 2 also underlines the importance of the maximum energy of the proton injection spectrum. In this calculation we use an exponential cut-off with  $E_{max} = 10^{21.5}$  eV. Assuming an  $E_{max}$  of  $10^{21}$  eV would not drastically decrease the neutrino flux, but any smaller value would.

Cutting off the proton injection spectrum at lower energy would, however, require very nearby sources for the extremely high energy showers detected by the Fly's Eye and AGASA experiments.

#### IV. NEUTRINOS FROM PROTON PROPAGATION OVER COSMOLOGICAL DISTANCES

In the following we will focus on the case of uniformly distributed sources with identical proton injection spectra. Although a homogeneous source distribution is disfavored by the resulting source energy requirements and arrival proton spectra [17,20], it serves here as a simple generic model whose results can be easily rescaled to account for local density enhancements or even nearby point sources.

The local neutrino flux of flavor  $i$  generated from the propagation of cosmic rays over cosmological distances can be written as

$$\begin{aligned} \mathcal{F}_i(E_{\nu_i}) &= \frac{dN_{\nu_i}}{d \ln E_{\nu_i} dt dA d\Omega} \\ &= \int \frac{\mathcal{L}(z)}{(1+z)4\pi[R(0)f(r)]^2} \frac{E_{\nu_i} dN_{\nu_i}}{dN_p dE_p^s dE_{\nu_i}} dE_p^s dV, \end{aligned} \quad (2)$$

with the scale factor  $R(z)$  and the volume element  $dV = R^3(z)f^2(r)drd\Omega$ . The source proton number luminosity per unit of comoving volume reads

$$\mathcal{L}(z) = \frac{dN_p}{dE_p^s dt^s dV} = \mathcal{H}(z)(1+z)^3 \mathcal{L}(0), \quad (3)$$

where  $\mathcal{H}(z)$  parametrizes the cosmological source evolution and the superscript  $s$  is used to label quantities measured in the source rest frame. Introducing the yield function

$$Y(E_p^s, E_{\nu_i}, z) = \frac{dN_{\nu_i}}{dN_p d \ln E_p^s d \ln E_{\nu_i}} \quad (4)$$

and rewriting Eq. (2) as redshift integral we obtain

$$\begin{aligned} \mathcal{F}_i(E_{\nu_i}) &= \int_0^{z_{max}} \mathcal{L}(z) \eta(z) \\ &\quad \times \int_{E_{thr}/(1+z)}^{E_{max}} Y(E_p^s, E_{\nu_i}, z) \frac{dE_p^s}{E_p^s} dz. \end{aligned} \quad (5)$$

The metric element  $\eta(z)$  is defined as

$$\begin{aligned} \eta(z) &= \frac{cdt}{dz} = \frac{c}{H_0} \frac{1}{1+z} [\Omega_M(1+z)^3 + \Omega_\Lambda \\ &\quad + (1 - \Omega_M - \Omega_\Lambda)(1+z)^2]^{-1/2} \end{aligned} \quad (6)$$

which simplifies to  $(1+z)^{-5/2} c/H_0$  for the Einstein - de Sitter universe ( $\Omega_M = 1, \Omega_\Lambda = 0$ ).

For source distances less than 200 Mpc ( $z \approx 0.05$ ) the neutrino yield function is calculated directly by Monte Carlo simulation, taking into account the change of the neutrino energy due to the propagation from the production place to earth,  $E_\nu = E_p^s/(1+z)$ . The yield function for larger distances is calculated on the basis of scaling arguments, neglecting the distance difference between the source and neutrino production locations as compared to the distance to Earth. The increase of the microwave background temperature with  $z$  and the neutrino energy loss due to the expansion of the universe lead to

$$Y(E_p^s, E_\nu, z) = Y(E_p^s(1+z), E_\nu, 0). \quad (7)$$

The cosmological evolution of the magnetic field is neglected. It does not play any significant role because of the fast decrease of the proton and neutron mean free path with redshift.

The source proton number luminosity  $\mathcal{L}(0)$  is parametrized as

$$\mathcal{L}(0) = P_0 \left( \int_{E_{\min}}^{E_{\max}} E_p^s \frac{dN_p}{dE_p^s} dE_p^s \right)^{-1} \frac{dN_p}{dE_p^s}, \quad (8)$$

with  $dN_p/dE_p^s$  given by Eq. (1) and  $P_0$  denoting the injection power per unit volume.

The injection power of cosmic rays with energy above  $E_{\min} = 10^{19}$  eV can be roughly estimated using the local cosmic ray energy density [21]. The cosmic ray flux  $dN/(dEd\Omega dAdt)$  at  $10^{19}$  eV is about  $2.5 \times 10^{-28}$   $\text{cm}^{-2}\text{s}^{-1}\text{ster}^{-1}\text{GeV}^{-1}$ . Assuming that:

- 1) all cosmic rays at that energy are extragalactic;
  - 2)  $10^{19}$  eV cosmic ray flux is as at injection; and
  - 3) the differential proton spectrum at injection is a power law with spectral index  $\alpha = 2$ ,
- one obtains a cosmic ray energy density

$$\rho_e = \frac{4\pi}{c} \int E \frac{dN}{dEd\Omega dAdt} dE \quad (9)$$

of  $1.1 \times 10^{54}$  erg/Mpc<sup>3</sup> per decade of energy. To calculate the injection power required to maintain this energy density one needs to make an assumption about the lifetime  $\tau_{CR}$  of these cosmic rays. A conservative approach would be to use a lifetime close to the Hubble time. Using  $\tau_{CR} = 10^{10}$  yrs gives a power of  $1.1 \times 10^{44}$  erg.Mpc<sup>-3</sup>yr<sup>-1</sup> per decade of energy. Of course, the total power for  $E > 10^{19}$  eV depends on the maximum energy at acceleration.

The correct way of calculating the injection power for a model of cosmic ray source distribution and injection (acceleration) spectra is to propagate the accelerated spectra from the sources to us and fit the locally observed spectrum. We do not perform this procedure because it involves assumptions on the cosmic ray source distribution and the structure and strength of the extragalactic magnetic fields which are beyond the scope of this paper. We use instead the cosmic ray power obtained in a

similar, somewhat simplified way by Waxman [22], who derived  $P_0 = 4.5 \pm 1.5 \times 10^{44}$  erg/Mpc<sup>3</sup>/yr between  $10^{19}$  and  $10^{21}$  eV for a variety of power law cosmic ray injection spectra. We will use this value in the calculation of the isotropic neutrino flux generated by the propagation of protons from homogeneously distributed cosmic ray sources, injected with the energy spectrum (1).

Finally we have to specify the cosmological evolution of the cosmic ray sources,  $\mathcal{H}(z)$ . We shall use the parametrization of [22], i.e.

$$\mathcal{H}(z) = \begin{cases} (1+z)^n & \text{for } z < 1.9 \\ (1+1.9)^n & \text{for } 1.9 < z < 2.7 \\ (1+1.9)^n \exp(-z/2.7) & \text{for } z > 2.7 \end{cases}, \quad (10)$$

with  $n = 3$  but will also briefly consider a stronger evolution with  $n = 4$ .

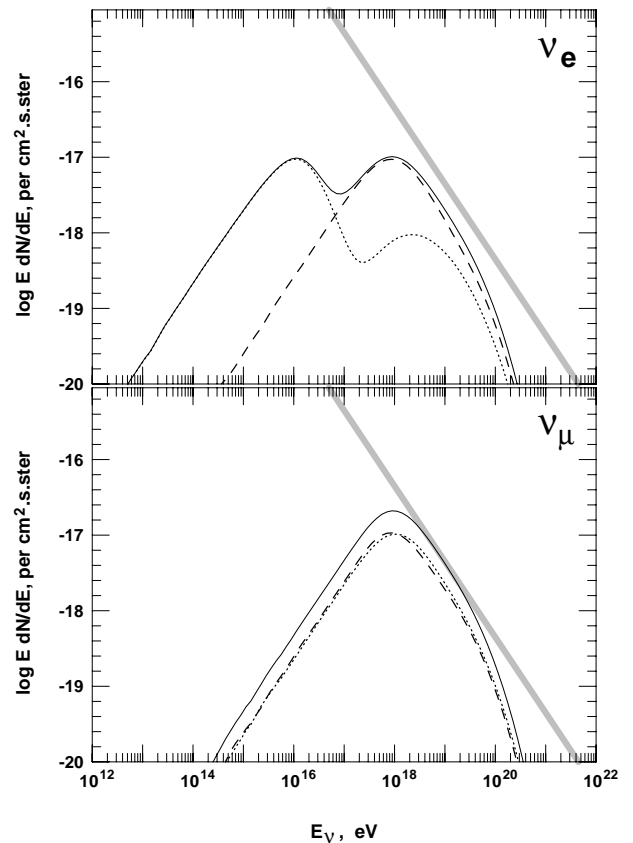


FIG. 3. Fluxes of electron neutrinos (dashed lines) and antineutrinos (dotted lines) generated in propagation of protons are shown in the upper panel. The lower panel shows the fluxes of muon neutrinos and antineutrinos. Solid lines show the sum of neutrinos and antineutrinos. The shaded line shows the Waxman & Bahcall [23,24] limit for neutrino production in cosmic ray sources which was derived using the same injection power and cosmological source evolution.

Fig. 3 shows electron and muon neutrino fluxes ob-

tained with  $n = 3$  for a homogeneous source distribution. The redshift integration was carried out to a maximum redshift of 4. An integration to higher redshifts does not increase the neutrino fluxes by more than 5%. The figure compares these fluxes with the Waxman & Bahcall [23,24] limit on neutrino production in cosmic ray sources, which is based on the same injection power  $P_0$ . Although the conditions in the source are much different from intergalactic space, such a comparison shows the expectations for ‘source’ versus ‘propagation’ neutrinos associated with UHECR of astrophysical origin. The muon neutrino flux calculated above is similar to the Waxman & Bahcall limit on the muon neutrino and antineutrino flux for energies between  $10^{18}$  and  $10^{19}$  eV. The reason is obvious: the limit is derived in the assumption of optically thin sources for the cosmic rays, i.e. each proton interacts at most once to generate neutrinos. Most of the protons with  $E_p > 10^{20}$  eV, on the other hand, interact more than once in propagation over cosmological distances. Compared to the photon fields at active galactic nuclei (AGN) or gamma-ray bursts (GRB) the microwave background photons are much softer, which keeps the proton interaction threshold, and the average neutrino energy, very high.

Unfortunately many parameters associated with the calculation of the neutrino fluxes as shown in Fig. 3 have rather large uncertainties. The power needed to maintain the flux of cosmic rays above  $10^{19}$  eV varies by about 30% for injection differential spectral indices between 1.8 and 2.7 [22]. The cosmological evolution of the source luminosity evaluated from star formation regions [25] could be somewhat stronger, as also indicated by the attempts to derive the cosmological evolution of GRB [26] and their fluences [27]. We show the influence on the generated neutrino fluxes in Fig. 4 where we calculate the neutrino flux with the same injection power but a stronger cosmological evolution -  $(1+z)^4$  up to  $z = 1.9$  and constant thereafter. We also show the neutrino fluxes obtained with the source evolution of Eq. (10) and differential injection spectral indices of 2.5 and 3, keeping again the injection power and  $E_{max}$  constant.

The stronger cosmological evolution increases the neutrino flux by a factor of 3 and generates a small shift of the maximum flux to lower energy. The integration was carried again to redshift of 4. If the constant source luminosity beyond  $z = 1.9$  continues to a redshift of 10, it would increase the neutrino flux by about 20%. The steeper injection spectra generate smaller neutrino fluxes, because of the much smaller number of protons above  $10^{20}$  eV that are mostly responsible for the neutrino production. The maximum of the neutrino fluxes is also shifted to lower energy for two different reasons, the steeper primary spectrum and the faster increase of the number of lower energy protons that interact at higher redshift.

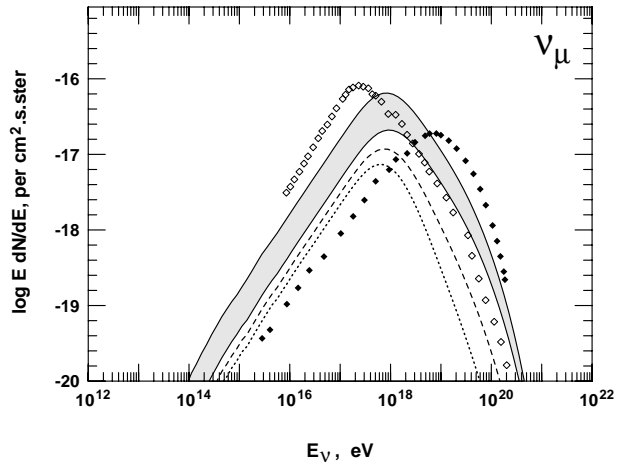


FIG. 4. The lower boundary of the shaded area corresponds to the neutrino flux shown in Fig. 3 with  $n = 3$  and the upper boundary is for  $n = 4$  up to  $z_{max}$  of 1.9. The dashed curve is for an injection spectrum of  $E^{-2.5}$  and the dotted curve is for  $E^{-3}$ . Open diamonds show neutrino fluxes calculated by Yoshida and Teshima [13] and the close diamonds are due to Stecker [12,28].

The two sets of points in Fig. 4 represent the calculations of Yoshida & Teshima (open diamonds,  $n = 4$ ,  $z_{max} = 4$ ) and of Stecker *et al.* [12,28] (full diamonds). Apart from the different normalization, these two calculations show peak neutrino energies different from the present calculation. Yoshida & Teshima predict a spectrum that peaks at lower energies. We understand this difference in terms of the overestimate of the proton photoproduction energy loss below  $10^{20}$  eV compared to the current calculation [18]. An additional decrease of the peak energy is related to the extension of the bright phase of the cosmic ray sources to a redshift of 4. The power normalization of Stecker *et al.* seems to be not much different from the normalization of Waxman. A description of the calculation was never published and we are not able to find the reason for the different position of the neutrino peak energy.

All results shown above are calculated for a homogeneous source distribution. It has been suggested many times in the past, and most recently in Ref. [29] that the observed cosmic ray spectrum can be best fit by a combination of a homogeneous source distribution with an enhancement of local (distance less than 20 Mpc) sources or with a single source at a similar distance.

Fig. 5 shows the neutrino fluxes generated under the assumption that the injection power of homogeneously distributed sources is  $P_0/2$  and 50% of the UHECR are generated by a single source at a distance of 20 Mpc. The difference between the neutrino flux magnitudes for a single source or local enhancement scenarios is very small and is not shown in the figure. The observational difference is very big because, for a single source scenario, all neutrinos would come from the direction of that source.

Most of the neutrinos due to proton propagation from a local source would be generated in the first interaction of protons of energy above  $10^{20}$  eV (see Fig. 2) that would not scatter significantly in a random extragalactic field with an average strength of less than 100 nG.

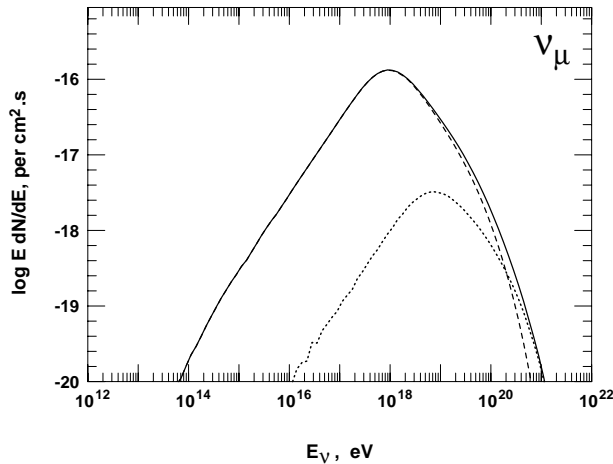


FIG. 5. Muon neutrino and antineutrino fluxes generated if one half of the local cosmic rays are generated by nearby (distance less than 20 Mpc) sources. Note that fluxes are given for the full solid angle of  $4\pi$ . The dashed curve corresponds to one half of the muon neutrino flux of Fig. 3, integrated over the full solid angle. The dotted line shows the production by locally generated cosmic rays by either a single source or by a local enhancement of the cosmic ray sources.

Finally we discuss the importance of the cosmological model. All calculations shown above are performed with the assumption of flat, mass dominated universe ( $\Omega_M = 1$ ). However, recent astrophysical observations agree better with models containing a cosmological constant  $\Lambda$  [30]. Since these observations support cosmologies in which the expansion accelerates, one expects an increased contribution to the neutrino production from higher redshifts.

Fig. 6 shows the difference in the expected neutrino fluxes for the Einstein – de Sitter Universe (solid line) and a model with  $\Omega_M = 0.3$  and  $\Omega_\Lambda = 0.7$ , as currently favored by measurements [31], and a source evolution proportional to  $(1+z)^4$ . We use the strongest possible source evolution and carry the integration out to a redshift of 8 to emphasize the difference between the cosmological models. For a flat universe the ratio of fluxes is always smaller than  $1/\sqrt{1-\Omega_\Lambda}$  (see Eq. (6)). The difference between the Einstein – de Sitter Universe and one with a non-vanishing cosmological constant does not, however, depend very strongly on the cosmological evolution model of the sources. The ratio between the two cosmologies is about 1.6 for  $n = 3$  evolution and 1.7 for  $n = 4$  evolution. One can compare the solid curves from Figs. 4 and 6 to see the increase of about 20% due to the

integration limits alone.

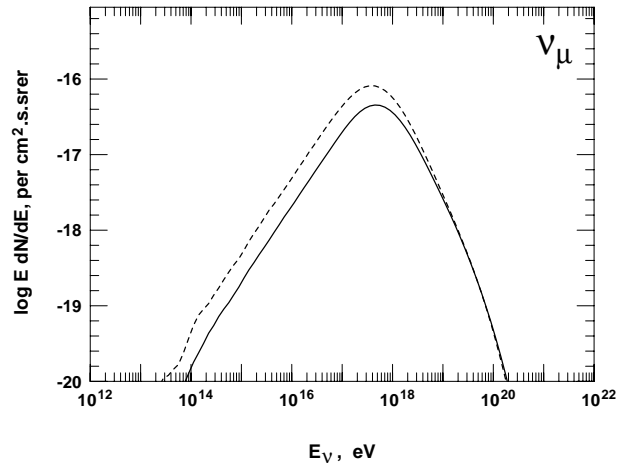


FIG. 6. Muon neutrino and antineutrino fluxes from homogeneous source distribution for the Einstein – de Sitter Universe (solid line) and for  $\Omega_\Lambda = 0.7$  (dashed line) for cosmological evolution  $(1+z)^4$  up to redshift of 1.9 and flat at higher redshifts.

## V. EVENT RATES FROM THESE NEUTRINOS

The peak energy of the neutrino spectra discussed above is well above  $10^{17}$  eV, the energy above which the whole Earth becomes opaque to neutrinos. The detection of these neutrinos by the upward going muons, generated by them in the rock surrounding deep underground (water or ice) detectors [32] is impossible because the absorption of the neutrinos in the Earth. Downgoing neutrino induced muons will be competing with atmospheric muons and the only detection technique left is the detection of neutrino induced hadronic and electromagnetic showers. Due to the small neutrino cross sections, detectors of  $\text{km}^3$  volume are required, which are currently proposed and designed [33,34]. In the following we estimate event rates for detecting high energy showers induced by neutrinos from proton propagation.

All types of neutrino interactions can generate showers. In charged current (CC) interactions of electron neutrinos and antineutrinos the neutrino energy is completely released in form of shower particles, since the hadronic shower that carries the fraction  $y$  of the initial neutrino energy  $E_\nu$  and the electromagnetic shower (with energy  $(1-y)E_\nu$ ) would not be distinguishable. In charged current interactions of muon neutrino and antineutrinos we only use  $yE_\nu$  as shower energy, as we do in the neutral current (NC) interactions of all neutrino types. We use the GRV98 [35] structure functions to calculate the neutrino cross sections at ultra-high energy. The resulting neutrino cross sections are very similar to those calculated by Quigg *et al.* [36] and Kwiecinski, Martin &

Stasto [37].

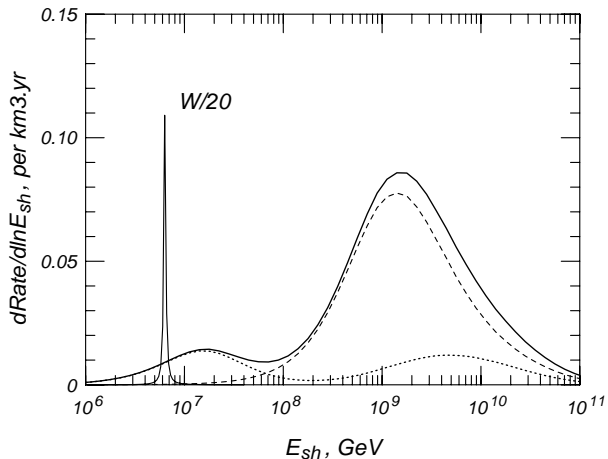


FIG. 7. Differential rates for showers initiated by charge current interactions of electron neutrinos (dashes) and antineutrinos (dots). The solid line gives the sum of those and the dash-dot lines gives the rate of the  $W^-$  resonance events.

Fig. 7 shows the differential rate for showers initiated by charged current interactions of electron neutrinos and antineutrinos for a cosmological source evolution with  $n = 3$ . The spike at  $E_\nu$  around  $8 \times 10^6$  GeV is the rate of  $W^-$  boson production by  $\bar{\nu}_e$ -electron interactions [38], divided by 20. The differential rate in the vicinity of the resonance is very high but the relevant energy range is small and the total rate is below 0.1 per  $\text{km}^3 \cdot \text{yr}$ . The total shower rate is dominated by  $\nu_e$  interactions around the peak energy of the neutrino flux.

The signal is thus dominated by  $10^9$  GeV and higher energy showers that do not have a significant background from cosmic ray interactions in the atmosphere or different neutrino sources.

TABLE I. Rates per  $\text{km}^3$  per year of showers above different energy generated by different types of neutrino interactions for  $P_0 = 4.5 \times 10^{44}$  erg/Mpc<sup>3</sup>/yr and a cosmological evolution with  $n = 3$  for homogeneously distributed cosmic ray sources (see text).

$\log E_{sh}$ (GeV) >	6	7	8	9	10
all $\nu$ , NC	0.32	0.28	0.20	0.07	0.01
$\nu_e$ , CC	0.33	0.32	0.29	0.20	0.04
$\nu_\mu + \nu_\tau$ , CC	0.56	0.50	0.36	0.13	0.02
$\tau$ decay	0.30	0.30	0.26	0.12	0.02
total	1.52	1.40	1.11	0.52	0.09

Table I gives the shower rates per  $\text{km}^3$  of water or ice per yr for showers generated by different types of neutrino interactions and different flavors. These rates are only approximate, because they represent  $d\sigma_\nu/dy$  folded with the flux of neutrinos reaching the detector and do not account for experimental efficiency and detector biases. They can only serve as a measure of the magnitude of the expected realistic event rates. Even so, the rates are low. Furthermore, these event rates correspond to the detected flux of UHECR with the assumptions that

- (i) the detected ultra-high energy cosmic rays are not produced by a single nearby source,
- (ii) the powerful sources of ultra-high energy cosmic rays are homogeneously distributed in the Universe, and
- (iii) our normalization of the power of the cosmic ray sources and the injection spectrum are correct.

In case that only a fraction of the UHECR comes from homogeneously distributed sources, these rates come down to the same fraction of the values presented in Table I. For the cosmological evolution model with  $n = 4$  the rates will go up by a factor of about 3. The assumption of a cosmological constant with  $\Omega_\Lambda = 0.7$  gives another moderate increase by a factor of 1.6 – 1.7.

The rates shown in Table I are calculated in the assumption that the atmospheric neutrino anomaly could indeed be explained by oscillations of  $\nu_\mu$  into  $\nu_\tau$  [39]. On the very long astrophysical pathlength 50% of the muon neutrinos would be converted to tau neutrinos. Charge current interactions of  $\nu_\tau$  would not be different from the  $\nu_\mu$  CC interactions, however, the generated  $\tau$  meson will decay, and about 3/4 of  $E_\tau$  would be released in hadrons that would initiate local showers. Table I gives the shower rates from  $\nu_\tau$  CC interactions and from  $\tau$  decays separately. This will be indeed true for the highest energy  $\tau$  mesons. The  $\tau$  decay length at an energy of  $10^8$  GeV is 4.9 km, i.e.  $\nu_\tau$  interaction and  $\tau$  decay will not be observable in the same  $\text{km}^3$  volume. At lower energy, however, the two showers may look like a single shower of higher energy, that would somewhat increase the numbers shown in the table.

## VI. DISCUSSION AND CONCLUSIONS

The biggest uncertainty in the magnitude of the neutrino fluxes from proton propagation is related to the distribution of cosmic ray sources. All arguments about the normalization of the cosmic ray injection power and the cosmological evolution of the cosmic ray sources are based on the assumption that the detected UHECR are of astrophysical origin and are not accelerated at a single nearby source. If the latter were the case, and the nearby source were responsible for all particles above  $10^{19}$  eV, we should have to restrict the source distance to less than 10 Mpc [18]. The local ultra-high energy cosmic ray density would then be much higher than the average cosmic ray density in the Universe. There will be, no doubts, other

regions where ultra-high energy cosmic rays are accelerated and are over-abundant. The overall normalization of the cosmic ray power would then depend on the filling factor of such regions. If one estimates this filling factor from the volume of the walls of galactic concentration, such as the supergalactic plane, that describes the galactic distribution within a redshift less than 0.05 [40], to nearby voids it will certainly not exceed 10%. In such a case the neutrino production due to proton propagation would be minimal as shown in Fig. 5 with the dotted line.

A correct estimate of the power in UHECR depends on the strength of the extragalactic magnetic field in our neighborhood. In case of an average strength of the turbulent field exceeding 1 nG, cosmic rays with an energy of about below  $10^{19}$  eV and below (with a gyroradius of less than 10 Mpc) will have diffusive propagation pattern, which will enhance their flux at Earth. On the other hand, regular extragalactic fields may guide these particles along the walls of matter concentration. All effects related to the propagation of UHECR should be a subject of further investigation before we could give a more reliable estimate of the UHECR power.

Recently several authors have argued that powerful astrophysical systems and potential cosmic ray sources, such as GRB, have a cosmological evolution stronger than  $(1+z)^3$  [27,41]. Ref. [27] presents a combined analysis of the far infrared luminosity as a tracer of the star formation rate [25] as a function of redshift and the gamma ray burst fluence. The star formation rate is fit with an exponential rise of  $\exp(2.9z)$  to a redshift of 1.7 and the GRB fluence distribution suggests a slow decrease at higher  $z$ . The use of such strong cosmological evolution and high activity at redshifts higher than 2 would place the estimate of the neutrino flux halfway between the two cosmological evolution models shown above.

Another very important factor is the injection spectrum of UHECR and the highest energy at acceleration,  $E_{max}$ . The qualitative picture of its influence is demonstrated in Figs. 2 and 4. Generally protons have to be accelerated to energies above  $10^{21}$  eV to generate significant neutrino fluxes from their propagation. In view of the observations of cosmic rays of energy significantly higher than  $10^{20}$  eV this is very likely if the sources of these particles are astrophysical objects.

Assuming homogeneously distributed astrophysical sources we obtain a neutrino flux similar to the Waxman & Bahcall limit at neutrino energies above  $10^{18}$  eV. This means that, with the assumptions and restrictions discussed above, one may expect similar fluxes of UHE neutrinos produced in astrophysical sources and in UHECR propagation.

Since the signature of these ultra-high energy neutrinos are showers, different types of air shower detectors should also be able to observe the highest end of the neutrino spectrum. The effective volume of the Auger observatory for UHE neutrino interactions was estimated to  $30 \text{ km}^3$  of water equivalent [42]. If this effective volume was achieved for a shower energy of  $10^{10}$  GeV, the Auger ob-

servatory would see about 3 events per year from the estimates shown in Table I. It is interesting to note that at an energy of  $10^9$  GeV the  $\tau$  decay length is of the order of the dimensions of the Auger observatory. ‘Double bang’ events, caused by  $\tau$  neutrinos as suggested by Learned & Pakvasa [43], could be detected if the sensitivity of the array was significant in this energy range.

Because of the extremely high effective volumes needed the proposed satellite air shower experiments EUSO and OWL [44,45] would be well suited for the observation of the ultra-high energy neutrino fluxes. For a rough estimate one could use the numbers from Table I. Because of the large field of view of these detectors they should be in principle able to observe ‘double bang’ events of energy above  $10^{19}$  eV.

Showers generated by ultra-high energy neutrinos could also be observed by their radio emission. There are proposals for such experiments [46] that may have an energy threshold of  $10^8$  GeV and a full effective volume of  $100 \text{ km}^3$ . Such detectors could take advantage of the higher shower rate that corresponds to the maximum of the neutrino flux as shown in Fig. 7.

The potential detection of ultra-high energy neutrinos is a crucial experimental result that will help us distinguish between an astrophysical (acceleration) and cosmological (top-down) origin of UHECR. In top-down scenarios the neutrino fluxes are primary, roughly equal to the gamma ray fluxes and at least an order of magnitude above the ultra-high energy nucleon fluxes. In all astrophysical scenarios the neutrinos, due to cosmic ray interactions at their sources or in propagation, are secondary and their flux is a fraction of the cosmic ray flux.

Measuring neutrinos from CR propagation can also help to distinguish between protons and heavy nuclei, such as iron, as highest energy cosmic rays. The energy loss of heavy nuclei during propagation over cosmological distances is governed by photo-disintegration. The absorption of photons leads mainly to giant dipole resonance excitation of the nuclei and, with a high probability, subsequently to the emission of a single nucleon in the de-excitation process [47]. Hence the neutrino spectrum is expected to be dominated by relatively low-energy neutrinos ( $E_\nu \lesssim 10^7$  GeV) from the beta decay of neutrons and unstable nuclei.

Finally it should be mentioned that the magnitude of the flux and the arrival direction of UHE neutrinos are a good indication of the cosmic ray source distribution in astrophysical scenarios.

## ACKNOWLEDGMENTS

The authors acknowledge helpful discussions with T.K. Gaisser. The research of TS is supported in part by NASA Grant NAG5-7009. RE is supported in part by the US Department of Energy contract DE-FG02 91ER 40626. These calculations are performed on DEC AI-

pha and Beowulf clusters funded by NSF grant PHY–9601834.

- 
- [1] K. Greisen, *Phys. Rev. Lett.* **16**, 748 (1966); G.T. Zatsepin & V.A. Kuzmin, *JETP Lett.* **4**, 78 (1966).
- [2] V.S. Berezinsky & G.T. Zatsepin, *Phys. Lett.* **28b**, 423 (1969); *Sov. J. Nucl. Phys.* **11**, 111 (1970).
- [3] J. Wdowczyk, W. Tkaczyk & A.W. Wolfendale, *J. Phys A5*, 1419 (1972).
- [4] F.W. Stecker, *Astroph. Space Sci.* **20**, 47 (1973).
- [5] V.S. Berezinsky & A.Yu. Smirnov, *Astroph. Space Sci.* **32**, 461 (1975).
- [6] V.S. Berezinsky & G.T. Zatsepin, *Sov. J. Uspekhi*, **20**, 361 (1977).
- [7] F.W. Stecker, *Astrophys. J.* **238**, 919 (1979).
- [8] C.T. Hill & D.N. Schramm, *Phys. Rev. D***31**, 564 (1985).
- [9] C.T. Hill, D.N. Schramm & T.P. Walker, *Phys. Rev. D***34**, 1622 (1986).
- [10] G. Cunningham *et al.*, *Astrophys. J.* **236**, L1 (1980).
- [11] R.M. Baltrusaitis *et al.*, *Phys. Rev. Lett.* **54**, 1875 (1985).
- [12] F.W. Stecker *et al.*, *Ap. J.* **410**, L71 (1993).
- [13] S. Yoshida & M. Teshima M., *Progr. Theor. Physics* **89**, 833 (1993).
- [14] M. Nagano & A.A. Watson, *Rev. Mod. Phys.*, **72**, 690 (2000).
- [15] D. Bird *et al.*, *Ap. J.*, **441**, 144 (1995).
- [16] N. Hayashida *et al.*, *Phys. Rev. Lett.* **73**, 3491 (1994).
- [17] A. Bhattacharjee & G. Sigl, *Phys. Rep.*, **327**, 109 (2000).
- [18] T. Stanev *et al.*, *Phys. Rev. D*, **62** 093005 (2000).
- [19] A. Mücke *et al.*, *Comp. Phys. Comm.* **124**, 290 (2000).
- [20] A.V. Olinto, *Phys. Rept.* **333-4**, 329 (2000).
- [21] T.K. Gaisser, *astro-ph/0011525*.
- [22] E. Waxman, *Ap. J.* **452**, L1 (1995).
- [23] E. Waxman & J. Bahcall, *Phys. Rev. D***59**, 023002 (1999).
- [24] J. Bahcall & E. Waxman, *astro-ph/9902383*.
- [25] P. Madau *et al.*, *Mon. Not. R. Astr. Soc.* **238**, 1388 (1996).
- [26] M. Schmidt, *Ap. J.* **523**, L117 (1999); E.E. Fenimore & E. Ramirez–Ruiz, *astro-ph/0004176*.
- [27] G. Pugliese *et al.*, *Astron. Astrophys.*, submitted, *astro-ph/0003025*.
- [28] D.N. Cline & F.W. Stecker, *0003459*.
- [29] M. Blanton, P. Blasi & A.V. Olinto, *Astropart Phys*, submitted, *astro-ph/0009466*.
- [30] N.A. Bahcall *et al.*, *Science*, **1481** (1999).
- [31] S.M. Carroll, *astro-ph/0004075*.
- [32] T.K. Gaisser & T. Stanev, *Phys. Rev. D***31**, 2770 (1985).
- [33] F. Montanet, *Nucl. Phys. Proc. Suppl.* **87**, 436 (2000).
- [34] The current status of the ICECUBE project is displayed at *pheno.physics.wisc.edu/icecube/*.
- [35] M. Glück, E. Reya & A. Vogt, *Eur. Phys. J. C***5**, 461 (1998).
- [36] R. Gandhi *et al.* *Phys. Rev. D***58**, 093009 (1998).
- [37] J. Kwiecinski, A.D. Martin and A.M. Stasto, *Phys. Rev. D***59**, 093002 (1999).
- [38] S.L. Glashow, *Phys. Rev.* 118B, 316 (1960).
- [39] T. Kajita & Y. Totsuka, ICR–REPORT–463–2000–7, *Rev. Mod. Phys.*, submitted.
- [40] O. Lahav *et al.*, *Mon. Not. R. Astr. Soc.* **312**, 166 (2000).
- [41] S.T. Scully & F.W. Stecker, *astro-ph/0006112*.
- [42] K.S. Capelle *et al.*, *Astropart. Phys.* **8**, 321 (1998)
- [43] J.G. Learned & S. Pakvasa, *Astropart. Phys.* **3**, 267 (1995).
- [44] The current status of the EUSO proposal is displayed at *www.ifcai.pa.cnr.it*.
- [45] L. Scarsi *et al.* in Proc. 26th ICRC (Salt Lake City), **2**, 384 (1999).
- [46] D. Besson *et al.* in Proc. 26th ICRC (Salt Lake City), **2**, 467 (1999).
- [47] J. P. Rachen, PhD-thesis, MPIFR Bonn, Germany, 1996.